Supplementary information to be published electronically for the paper: "A water soluble Mn(II) polymer with aqua metal bridges"

Mònica Fontanet,[a] Montserrat Rodríguez, [a] Isabel Romero,* [a] Xavier Fontrodona, [a] Francesc Teixidor,*, [b] Clara Viñas,[b] Núria Aliaga-Alcalde, [c] Pavel Matějíček.[d]

[a] *Departament de Química, Institut de Química Computacional and Serveis Tècnics de Recerca, Universitat de Girona, Campus de Montilivi, E-17071 Girona, Spain. Fax: +34 972 418150; Tel: +34 972 418262;E-mail: marisa.romero@udg.edu*
[b] *Institut de Ciencia de Materials de Barcelona, ICMAB-CSIC*
Campus UAB, E-08193 Bellaterra, Spain;E-mail: teixidor@icmab.es
[c] *Universitat de Barcelona, Diagonal 645, E-08028 Barcelona, Spain;* ICREA, *Passeig Lluis Companys 23, 08010 Barcelona, Spain.*
[d]*Department of Physical and Macromolecular Chemistry; Faculty of Science; Charles University in Prague, Hlavova 2030, 128 40 Prague 2, Czech Republic*

1. Experimental Details

2. Spectroscopic properties

3. Crystal structures and data of 1 and 2.

4. Structure Refinement Comments

5. Magnetic properties.

6. Dynamic Light Scattering (DLS)

1. Experimental Details

Materials. All reagents used in the present work were obtained from Aldrich Chemical Co and were used without further purification. Reagent grade organic solvents were obtained from SDS and high purity de-ionized water was obtained by passing distilled water through a nano-pure Mili-Q water purification system.

Instrumentation and Measurements. FT-IR spectra were taken in a Mattson-Galaxy Satellite FT-IR spectrophotometer containing a MKII Golden Gate Single Reflection ATR System. Elemental analyses were performed using a CHNS-O Elemental Analyser EA-1108 from Fisons. ESI-MS spectra have been performed in a Thermo Quest Finnigan Navigator LC/MS cromatograph. NMR spectra have been recorded with a Bruker ARX 300 or a DPX 400 instrument equipped with the appropriate decoupling accessories $^{1}H\{^{11}B\}$ NMR (300.13/400.13 MHz), and $^{11}B\{^{1}H\}$ NMR (96.29/128.37 MHz) spectra were recorded in D_2O. Chemical shift values for ^{11}B NMR spectra were referenced to external $BF_3 \leftarrow OEt_2$ and those for $^{1}H\{^{11}B\}$ spectra were referenced to SiMe4. Chemical shifts are reported in units of parts per million downfield from reference, and all coupling constants in Hz.

Magnetic Susceptibility Studies. Magnetic susceptibility measurements between 2.0 – 300.0 K were carried out in a SQUID magnetometer Quantum Design Magnetometer, model MPMP. Susceptibility measurements were performed using a field of 1.0 T. Pascal's constants were used to estimate the diamagnetic corrections for the compound. The fit was performed by minimizing the function $R = \Sigma(\chi MT)exp - (\chi MT)calc]2/\Sigma (\chi MT)exp]2$.

Microscopy Studies

Cryo-TEM. The studies were performed by using a Jeol JEM-1400 electron microscope operating at 120 kV and equipped with a CCD multiscan camera (Gatan). The microscope was equipped with a Gatan cryoholder and the samples were maintained at -177ºC during imaging. Micro drops (2 μL) of the water solutions of amphiphiles were blotted onto holey carbon grids (Quantifoil) previously glow discharged in a BAL-TEC MSC 010 glow discharger unit, which were immediately plugged into liquid ethane at -180 ºC using a Leica EM CPC cryoworkstation.

Scattering Studies

Dynamic Light Scattering (DLS) and Static Light Scattering (SLS). The light scattering setup (ALV, Langen, Germany) consisted of a 633 nm He-Ne laser, an ALV CGS/8F goniometer, an ALV High QE APD detector, and an ALV 5000/EPP multibit, multitau autocorrelator. DLS data analysis was performed by fitting the measured normalized intensity autocorrelation function g2(t) = 1 + β|g1(t)|2, where g1(t) is the electric field correlation function, t is the lag-time and β is a factor accounting for deviation from the ideal correlation. An inverse Laplace transform of g1(t) with the aid of a constrained regularization algorithm (CONTIN) provides the distribution of relaxation times, τA(τ). Effective angle- and concentration-dependent hydrodynamic radii, $R_H(q,c)$, were obtained from the mean values of relaxation times, $\tau_m(q,c)$, of individual diffusive modes using the Stokes-Einstein equation. The SLS data were treated by the standard Zimm or Berry method. As the refractive index increment is unknown, SLS scattering curves were used only for calculation of radius of gyration Rg.

Samples for DLS measurements were dissolved in deionized water in concentration range 0.0169 – 24.8 g/L, where solutions of lower concentrations were typically prepared by dilution of the stock solution by filtered water. Solutions in diethyl ether and dichloromethane with concentrations about 1 g/L were also prepared. In case of dichloromethane, few droplets of water had to be added in order to obtain a clear solution. For combined SAXS/WAXS experiments, aqueous solutions with weight fractions of the sample 1.0%, 2.8% and 9.0% were prepared.

X-ray structure determination

Measurement of the crystals were performed on a Bruker Smart Apex CCD diffractometer using graphite-monochromated Mo Kα radiation (λ = 0.71073Å) from an X-Ray tube. Data collection, Smart V. 5.631 (BrukerAXS 1997-02); data reduction, Saint+ Version 6.36A (Bruker AXS 2001); absorption correction, SADABS version 2.10 (Bruker AXS 2001) and structure solution and refinement, SHELXTL Version 6.14 (Bruker AXS 2000-2003). The crystallographic data as well as details of the structure solution and refinement procedures are reported in Table 1 and 2. CCDC 907977 (1), and 907978 (2), contain the supplementary crystallographic data for this paper. These data can be obtained free of charge from The Cambridge Crystallographic Data Centre via www.ccdc.cam.ac.uk/products/csd/request/

Preparations. The 1-CH_3-2-CO_2H-1,2-closo-$C_2B_{10}H_{10}$ ligand[l] was prepared according to literature procedures.

Synthesis of [Mn(μ-H_2O)(μ-1-CH_3-2-CO_2-1,2-closo-$C_2B_{10}H_{10})_2]_n$. $(H_2O)_n$, 1.

To a suspension of 0.249 g (1.233 mmols) of 1-CH3-2-CO2H-1,2-closo-C2B10H10 in 20 mL of water was added 0.142 g (1.233 mmols) of MnCO3 in 5 mL of water. The solution was stirred and heated to 40 ˚C for 2h. Afterward, the solution was filtered and the solvent was removed under vacuum to obtain a white solid. The latter was crystallized by slow evaporation of a dichloromethane solution. Yield: 0.274g (94%). 1H{11B} NMR (400.13 MHz, D2O , 25˚C): δ= 2.33 (br s, B-H), 2.20 (br s, B-H), 2.10 (br s, B-H), 2.03 (br s, B-H), 1.96 (br s, B-H), 1.93 (s, CH3). 11B{1H} NMR (128.37, D2O, 25˚C): δ= -4.1 (1J(B,H)= 148.9, 2B), -7.0 (1J(B,H)= 150.3, 2B), -10.10 (1J(B,H)= 118.1, 3B), -10.93 (1J(B,H)= 142.5, 3B) . Anal. Found (calcd.) (%) for C8H28O5B20Mn: C 20.24(20.21); H 5.81(5.94).IR(cm-1):ν = 3631, 3381ν(OH), 3208 ν(CH3), 2583 ν (B-H), 1619, 1569 ν(COO-)as, 1379 ν(COO-)sim, 1193, 1148, 844 δ(O-H), 725 υ(B-C).

Synthesis of [$Mn_3(H_2O)_4$(μ-1-CH_3-2-CO_2-1,2-closo-$C_2B_{10}H_{10})_6(C_4H_{10}O)_2$], 2.

By recrystallization of 1 in a diethyl ether solution and then slow diffusion of pentane into this solution, colouorless needles suitable for X-ray diffraction were obtained corresponding to complex 2

2. Spectroscopic properties

The IR spectrum of **1** displays the typical υ(B-H) absorption at 2583 cm^{-1}, characteristic of *closo* carborane derivatives.[2] The difference between the frequencies of the symmetric and antisymmetric stretches for the carboxylate ligands (1569 $\nu(COO^-)_{as}$, 1379 $\nu(COO^-)_{sym}$), lies within the ranges quoted for bidentate bridging ligands.[3] The study of the polymeric structure in water solution has been performed by $^1H\{^{11}B\}$-, $^{11}B\{^1H\}$- NMR, ESI-MS spectroscopy, cryo-TEM microscopy and Dynamic Light Scattering (DLS). The $^1H\{^{11}B\}$- and $^{11}B\{^1H\}$-NMR spectra of **1** fully agree with the solid structure confirmed by X-ray crystallography. It can be observed that the $^1H\{^{11}B\}$-spectrum exhibits a resonance at 1.93 ppm attributed to the C_c-CH_3 protons. The resonances of the protons bonded to the B atoms appear as broad singlets over a wide chemical shift range in the region from 0 to +3 ppm. The $^{11}B\{^1H\}$-NMR resonances for all complexes featured similar patterns in the range from -4.1 to -11 ppm that agree with a *closo* cluster.[4] ESI-MS spectrum of the polymer in water in the scan region 500 m/z to 2000 m/z shows different peaks that could be assigned to the $\{[Mn(L)_2(H_2O)]_4 + H^+\}$ fragment (m/z 1902,8) and $\{[Mn(L)_2(H_2O)]_3 + LH + H^+\}$ fragment (m/z 1628,6) together with other peaks of less intensity corresponding to the $\{[Mn(L)_2(H_2O)]_2 - (L) + 2H^+\}$ fragment (m/z 795,6) and $\{[Mn(L)_2(H_2O)]_2 - (LH) + Na^+\}$ fragment (m/z 772,6)

3. Crystal structures and data of 1 and 2.

Table S1. Crystal Data for X-ray structures of **1** and **2**.

	1	**2**
Empirical formula	$C_8H_{30}B_{20}O_6Mn$	$C_{48}H_{146}B_{60}O_{22}Mn_3$
Formula weight	491.44	1889.07
Crystal system	Orthorhombic	Triclinic
Space group	Pna21	P-1
a [Å]	13.21(2)	14.5473(14)
b [Å]	28.04(4)	14.7700(14)
c [Å]	7.569(12)	15.5876(15)
α [°]	90	63.6570(10)
β [°]	90	74.414(2)
γ [°]	90	67.632(2)
V [Å3]	2804(8)	2755.4(5)
Formula Units/Cell	4	1
ρcalc. [g cm-3]	1.164	1.138
μ [mm-1]	0.493	0.392
R1[a], [I > 2σ(I)]	0.0788	0.0625
wR2[b] [all data]	0.1943	0.1821

[a] $R_1 = \sum||F_o| - |F_c||/\sum|F_o|$. [b] $wR_2 = [\sum\{w(F_o^2-F_c^2)^2\}/\sum\{w(F_o^2)^2\}]^{½}$, where $w = 1/[\sigma^2(Fo^2) + (0.0042P)^2]$ and $P=(F_o^2+2F_c^2)/3$

Table S2. Selected bond lengths (Å) and angles (°) for complexes **1** and **2**.

	1		**2**		**2**
Mn(1)-O(2)	2.115(9)	Mn(1)-O(1)	2.129(2)	O(7)-Mn(1)-O(8)	92.72(9)
Mn(1)- O(4)	2.133(8)	Mn(1)- O(3)	2.136(2)	O(1)-Mn(1)-O(9)	90.16(8)
Mn(1)-O(3)	2.154(9)	Mn(1)-O(5)	2.151(2)	O(3)-Mn(1)-O(9)	90.95(9)
Mn(1)-O(1)	2.187(9)	Mn(1)-O(7)	2.157(2)	O(5)-Mn(1)-O(9)	84.69(8)
Mn(1)-O(5)#1	2.302(11)	Mn(1)-O(8)	2.194(2)	O(7)-Mn(1)-O(9)	87.03(9)
Mn(1)-O(5)	2.338(13)	Mn(1)-O(9)	2.346(2)	O(8)-Mn(1)-O(9)	176.93(8)
O(2)-Mn(1)-O(4)	92.4(4)	Mn(2)-O(4)	2.1179(19)	O(4)-Mn(2)-O(4)#1	180.00(13)
O(2)-Mn(1)-O(3)	88.9(4)	Mn(2)-O(4)#1	2.1179(19)	O(4)-Mn(2)-O(2)	90.79(9)
O(4)-Mn(1)-O(3)	177.1(6)	Mn(2)-O(2)	2.1528(18)	O(4)#1-Mn(2)-O(2)	89.21(9)
O(2)-Mn(1)-O(1)	179.2(6)	Mn(2)-O(2)#1	2.1528(18)	O(4)-Mn(2)-O(2)#1	89.21(9)
O(4)-Mn(1)-O(1)	88.1(4)	Mn(2)-O(9)#1	2.228(2)	O(4)#1-Mn(2)-O(2)#1	90.79(9)
O(3)-Mn(1)-O(1)	90.5(4)	Mn(2)-O(9)	2.228(2)	O(2)-Mn(2)-O(2)#1	180.00(12)
O(2)-Mn(1)-O(5)#1	84.2(4)	O(1)-Mn(1)-O(3)	92.64(9)	O(4)-Mn(2)-O(9)#1	85.76(9)
O(4)-Mn(1)-O(5)#1	88.1(4)	O(1)-Mn(1)-O(5)	173.32(8)	O(4)#1-Mn(2)-O(9)#1	94.24(9)
O(3)-Mn(1)-O(5)#1	89.5(4)	O(3)-Mn(1)-O(5)	91.70(9)	O(2)-Mn(2)-O(9)#1	91.10(8)
O(1)-Mn(1)-O(5)#1	95.3(4)	O(1)-Mn(1)-O(7)	87.95(9)	O(2)#1-Mn(2)-O(9)#1	88.90(9)
O(2)-Mn(1)-O(5)	95.7(4)	O(3)-Mn(1)-O(7)	177.89(9)	O(4)-Mn(2)-O(9)	94.24(9)
O(4)-Mn(1)-O(5)	91.7(4)	O(5)-Mn(1)-O(7)	87.54(9)	O(4)#1-Mn(2)-O(9)	85.76(9)
O(3)-Mn(1)-O(5)	90.8(3)	O(1)-Mn(1)-O(8)	92.89(9)	O(2)-Mn(2)-O(9)	88.90(8)
O(1)-Mn(1)-O(5)	84.8(4)	O(3)-Mn(1)-O(8)	89.28(9)	O(2)#1-Mn(2)-O(9)	91.10(8)
O(5)#1-Mn(1)-O(5)	179.7(4)	O(5)-Mn(1)-O(8)	92.24(8)	O(9)#1-Mn(2)-O(9)	180.0

Figure S1. X-ray structure of **1** showing the polymeric chains and hydrogen bonding connecting the hydration water with the polymeric chain.

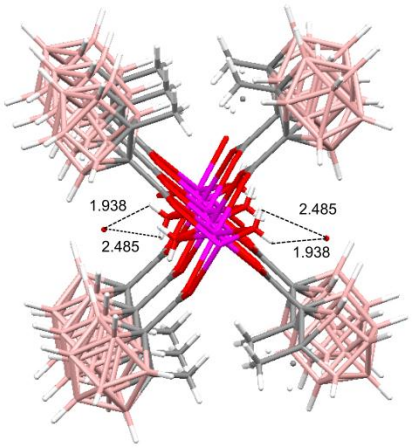

Figure S2. Packing diagram for the “chiral layers“ of polymer 1

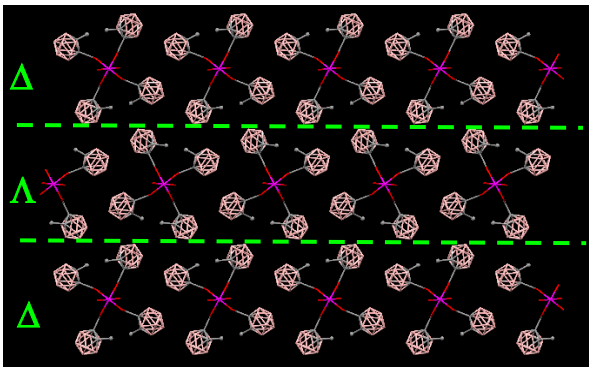

The packing structure of polymer **1** that displays polymeric chiral chains because the methyl group of the carboranylcarboxylate ligand is shifted respect to the center of the coordinated carboxylate group. Then, two different conformations for these chains (lambda and delta) can be found, which have been shown in Figure S3a. In this figure each methyl group is oriented toward the methyl group of a neighboring ligand, with a C⋯C distance of 2.66 Å. Moreover, the orientation of all methyl groups is the same within a chain, and opposite to the methyl groups from a different chain. The imaginary helical path defined by the positions of the methyl groups along each polymeric chain allows to assign them either the Δ or Λ conformation. The chains are spatially arranged in the network so that they define a sort of "chiral layers" conformed by adjacent chains having the same conformation. Figure S3b shows the packing structure of these “chiral layers” that lead to a 2D structure. It can be concluded that this polymer is formed by a sequence of chiral chains due to the orientation of the methyl groups from the carboranylcarboxylate ligands.

3. Structure Refinement Comments.

CCDC 907977 (mfcl13, C8 H28 B20 Mn O5, H2O)

Check-cif Suggests Possible Pseudo/New Space-group Pnma. The Pnma S.G. was tested. Trying to refine the structe in Pnma was unsuccesful because that made the molecule adopts a higher symmetry than it can has.

The hydrogen atoms associated with the solvent water could not be located in the Difference Fourier map and so are omitted from the final refinement and structure factor calculations. They are, however, included in the reported chemical formula and derived values (e.g. formula weight, F_000, etc).

The H-atoms were placed in geometrically optimized positions and forced to ride on the atom to which they are attached. The OH2 hydrogens of the water molecule coordinated to the metal atom were refined on the riding model with O-H distance free to refine.

The thermall ellipsoids are ellongated, with large Ueq for several atoms.
All the atoms types were checked to be the correct ones.

Boron-Boron distance for B1-B2, B2-B3, B2-B8, have been restarined to 1.70(2) Å, and Boron-Boron distance for B11-B12, B11-B17, B12-B13, B12-B16, B13-B14, B13-B15, B13-B16, B14-B15, B14-B19, B15-B16, B15-B19, B15-B20, B16-B17, B16-B20, B17-B18, B17-B20, B18-B19, B18-B20, B19-B20, have been restarined to 1.700(1) Å using the dfix instruction in shelxtl

The carbon-boron distance in C7-B11, C7-B14 are restrained to 1.60(2) Å using the dfix instruction in shelxtl

The carbon-carbon distance in C3-C4, C3-C4', C7-C8' are restrained to 1.54(2) Å using the dfix instruction in shelxtl

The Uij components of the disordered atoms c8 c8' and c4 c4' were restrained to a isotropic behavior using the Isor instruction in shelxtl

CCDC 907978 (mfcmn, C48 H146 B60 Mn3 O22)

C-H Hydrogen atoms were placed in calculated positions and included as riding contributions with isotropic displacement parameters 1.2 or 1.5 times those of the attached atom for C-H2 and C-H3 respectively.

The B-H and O(7) OH2 Hydrogen atoms were placed in calculated positions and included as riding contributions with isotropic displacement parameters 1.2 those of the attached atom.

The bridging O(9) OH2 hydrogen atoms were located in the difference fourier map and refined freely.

The C3y-C4y distance has been restrained to 1.540(1) Å using the dfix instruction in shelxtl.

4. Magnetic properties.

Magnetic structural correlations were performed for compound **1.** As described above, **1** is a novel 1D Mn^{II} assembly, in which the metallic ions are linked by two [1-CH_3-2-CO_2-1,2-closo-$C_2B_{10}H_{10}]^-$ ligands and one H_2O molecule. In the crystal, all Mn···Mn distances are equivalent, therefore the system could be magnetically described just using one exchange coupling, *J*. Plots showing the thermal evolution of the magnetic molar susceptibility, χ_M and $\chi_M T$ are shown in Figure S3. These solid-state, variable-temperature (2.0- 300 K) data were collected on polycrystalline samples using 0.02 T (from 2 to 30 K) and 0.3 T (from 2 to 300 K) fields.

The $\chi_M T$ data at room temperature (4.47 cm^3 mol^{-1} K) agrees well with the spin-only value expected for a high-spin Mn^{II} ion (4.375 cm^3 mol^{-1} K when g = 2). The magnetic answer decreases continuously from 300 K down to 50 K, and then rapidly upon further cooling. This behavior is indicative of a weak antiferromagnetically coupled system and it is also portrayed in the χ_M vs T graph. The magnetic molar susceptibility displays a maximum at 5 K and decreases very quickly afterwards (Figure 3S). The interaction through the triple bridge was evaluated by the modified expression for a classical Heisenberg chain, derived by Fisher, based on the exchange *H*amiltonian $H = -J\Sigma S_i S_{i+1}$.[5] The best fit parameters were found for J = -0.91 cm^{-1}, g = 2.01, TIP of 80×10^{-6} cm^3 mol^{-1} and R = 8×10^{-5}.

Figure S3. Experimental data including χ_M vs T (y axis on the left side) and $\chi_M T$ vs T (y axis on the right side) of 1 between 2.0 and 300.0 K. The experimental points are shown as black squares and the red and blue lines correspond to the theoretical values, also in that order.

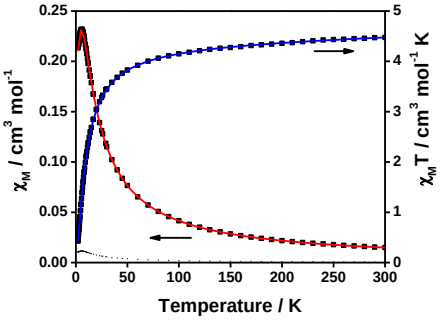

The water bridge and syn-syn arrangement of the two carboxylate ligands lead the magnetic answer of this new array providing a good overlap of magnetic orbitals and therefore displaying antiferromagnetic behavior. The weakness of the coupling has been already observed in similar aqua-bridged MOFs[6,7] and dinuclear complexes, where Mn-O_{H2O} and $Mn^{II}\cdots Mn^{II}$ distances are relatively long and the Mn-(OH_2)-Mn angle is always higher than 108 ° (Table S3). The coupling through the water bridge has been proven even weaker than the coupling observed for OH- and OR-bridged species (strength order: O_2^- > OH^- > H_2O).[8, 9]

Table S3. Crystallographic and magnetic comparison between complex **1** and previous literature works.

	1**	2	3*	4	5 *	6 *	7 *	8
Mn…Mn (Å)	3.785	3.512	3.777	3.756	3.595	3.621	3.618	3.77
Mn-(OH_2)-Mn(°)	109.6	-	114.4	114.9	110.2	110.0	108.3	114.4
Mn-OH_2 (Å)	2.321	2.262	2.246	2.227	2.182	2.215	2.252	2.246
	2.309				2.203	2.205	2.111	
g	2.01	-	1.97	-	1.939	2.012	2.0	-
J (cm^{-1})	-0.91	-	-1.26	-	-2.73	2.952	-1.0	-

* $H = -2JS_iS_{i+1}$. ** Number **1** corresponds to this work where $H = -JS_iS_{i+1}$.

5. Dynamic Light Scattering (DLS)

Figure S4. Concentration dependence of hydrodynamic radius of nanoparticles in aqueous solutions of "polymer" measured at scattering angle 90deg

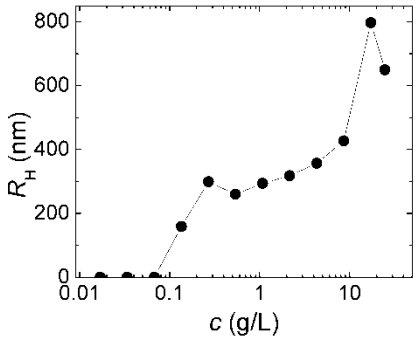

Figure S5. Distribution of hydrodynamic radii of nanoparticles in aqueous solutions of "polymer" at scattering angle 90deg for different concentrations as indicated in graph.

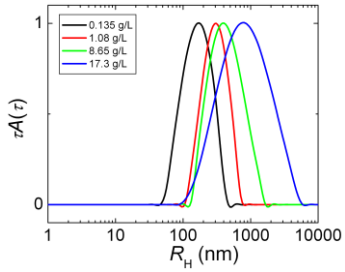

[1] U. Venkatasubramanian, D.J. Donohoe, D. Ellis, B.T. Giles, S.A. Macgregor, S. Robertson, G.M. Rosair, A.J. Welch, A.S. Batsanov, L.A. Boyd, R.C.B. Copley, M.A. Fox, J.A.K. Howard, K.. Wade, *Polyhedron*, **2004,** 23, 629-636.

[2] L.A. Leites, *Chem. Rev*. **1992**, 92, 279-323. .

[3] R.C. Mehrotra, R. Bohra, *Metal Carboxylates; Academic Press: New York*, **1983**, 396.

[4] L.J. Todd, A.R. Siedle, *Prog. Nucl. Mag. Reson. Spectrosc.*, **1979**, 13, 87-176.

[5] a) M.E. Fisher, *Am. J. Phys*. **1964**, 32, 343. b) O. Kahn, *Molecular Magnetism*, VCH, New York, **1993**, page 258.

[6] Su, Z.; Chen, S.-S.; Fan, J.; Chen, M.-S.; Zhao, Y.; Sun, W.-Y. Cryst. Growth. Des. **2010**, 10, 3675.

[7] Niu, C.-Y.; Zheng, X.-F.; Wan, X.-S.; Kou, C.-H. Cryst. Growth. Des. **2011**, 11, 2874.

[8] S-B. Yu, S.J. Lippard, I. Shweky, A. Bino, *Inorg. Chem*. **1992**, 31, 3502.

[9] a) Y-L. Shen, S.-L. Sun, W-D. Song, Acta Cryst. Section E, 2007, E63, m1309. b) B-H. Ye, T. Mak, I.D. Williams, X-Y. Li, *Chem. Commun.*, **1997**, 1813.(c) D. Coucouvanis, R.A. Reynolds III, W.R. Dunham, *J. Am. Chem. Soc*. **1995,** 117, 7570.(d) R.A. Reynolds III, W.R.; Dunham, D. Coucouvanis, *Inorg. Chem*. **1998**, 37, 1232. (e)B-H. Ye, I.D. Williams, X-Y. Li, J. *Inorg. Biochem*., **2002**, 92, 128.